

Mapping dust column density in dark clouds by using NIR scattered light : case of the Lupus 3 dark cloud

Yasushi NAKAJIMA, Ryo KANDORI, Motohide TAMURA

National Astronomical Observatory of Japan

Tetsuya NAGATA

Kyoto University

Shuji SATO

Nagoya University

and

Koji SUGITANI

Nagoya City University

October 26, 2018

Abstract

We present a method of mapping dust column density in dark clouds by using near-infrared scattered light. Our observations of the Lupus 3 dark cloud indicate that there is a well defined relation between (1) the $H - K_s$ color of an individual star behind the cloud, i.e., dust column density, and (2) the surface brightness of scattered light toward the star in each of the J , H , and K_s bands. In the relation, the surface brightnesses increase at low $H - K_s$ colors, then saturate and decrease with increasing $H - K_s$. Using a simple one-dimensional radiation transfer model, we derive empirical equations which plausibly represent the observed relationship between the surface brightness and the dust column density. By using the empirical equations, we estimate dust column density of the cloud for any directions toward which even no background stars are seen. We obtain a dust column density map with a pixel scale of 2.3×2.3 arcsec² and a large dynamic range up to $A_V = 50$ mag. Compared to the previous studies by Juvela et al., this study is the first to use color excess of the background stars for calibration of the empirical relationship and to apply the empirical relationship beyond the point where surface brightness starts to decrease with increasing column density.

1 Introduction

Dark clouds are seen as dark patches against bright star fields, while they are observed as reflection nebulae at near-infrared (NIR) wavelengths in the recent decade (Lehtinen & Mattila 1996, Nakajima et al. 2003, Foster & Goodman 2006). The images of NIR reflection nebulae give us an insight that darker areas with fewer background stars have larger column densities. In our previous paper (Nakajima et al. 2003), we showed that the Lupus 3 dark cloud appears as an NIR reflection nebula and suggested that there is a relationship between the NIR surface brightness and dust column density toward the Lupus 3 dark cloud. It is worth investigating whether if we can quantify the relationship between the NIR surface brightness and column density.

Star counting, color excess of background stars, molecular gas and thermal dust emissions have been used for column density mapping of dark clouds. Juvela et al. (2006) reviewed these methods intensively. Each of these methods has limitations. A common limitation to all these methods is that it is hard to obtain a high spatial resolution. Padoan et al. (2006) and Juvela et al. (2006) examined the use of scattered NIR surface brightness as a new high resolution tracer of the interstellar clouds. They derived an analytical formula to convert NIR surface brightness to visual extinction. The formula is linear at low visual extinctions and starts to saturate when visual extinction reaches ~ 10 mag. Juvela et al. (2006) used numerical simulations and radiative transfer calculations to show that the NIR surface brightness can be converted to column density in the range of $A_V < 15$ mag with accuracy of better than 20%. Juvela et al. (2008) applied the method to a filamentary cloud in Corona Australis. The method using surface brightness and one using color excess of background star agrees below $A_V \sim 15$ mag.

In this paper, we propose an empirical method of estimating column density of dark clouds up to $A_V \sim 50$ mag by using NIR surface brightness. We re-examine the NIR data of the Lupus 3 dark cloud in Nakajima et al. (2003) and

obtain a plausible empirical equations which fit the observed relationship between the surface brightness and column density. Using the relationship, we obtain the dust column density map from the surface brightness.

2 Data

We obtained the J , H , and K_s band data of the Lupus 3 dark cloud on 2001 June 4 and 7 with the IRSF 1.4 m telescope and the NIR camera SIRIUS. The total integration time was 135 minutes for each band. Procedures of observations and data reduction are almost the same as described in Nakajima et al. (2003). The differences are as follows. We included data obtained on 2001 June 7 in addition to those on 2001 June 4 to obtain a higher signal-to-noise ratio. We calibrated photometry by comparing stars in the observed field with 2MASS catalog stars instead of using standard stars. Color conversion factors between the 2MASS and IRSF/SIRIUS system were taken into account (Nakajima et al. 2008). Hence, magnitudes and colors are presented in the 2MASS photometric system. We selected well-measured stars by the sharpness value of ALLSTAR routine in IRAF¹. We rejected stars with an absolute value of sharpness larger than 0.2 as no point-like sources. The total number of the stars which were selected in both the H and K_s bands was 2910 and that in all the three bands was 1611. We corrected vertical streaks due to bright stars by comparing adjacent columns. We calculated the surface brightness toward each pixel by taking the median value of $5 \times 5 = 25$ pixels centered at the pixel after subtraction of stars by using SUBSTAR routine in IRAF. The pixel area corresponds to 2.3×2.3 arcsec², and the error was estimated by standard deviation of the 25 pixels. The 3-sigma limiting fluxes for surface brightness were $F_J = 1.1$, $F_H = 1.6$, and $F_{K_s} = 2.3 \mu\text{Jy arcsec}^{-2}$.

3 Results and Discussion

3.1 Surface brightness and column density

Surface brightness maps in the J , H , and K_s bands are shown in Figure 1. The values of A_V toward the background stars are shown in Figure 2. The A_V is estimated from the observed $H - K_s$ color of each background star by $A_V = 18.0 \times [(H - K_s) - (H - K_s)_{\text{intrinsic}}]$. The conversion factor between A_V and the color excess is calculated from the theoretical curve No. 15 of van de Hulst (1946, hereafter vdH).² Here, we set $(H - K_s)_{\text{intrinsic}} = 0.15$ for all the background stars, which is the average value of those behind the Lupus 3 dark cloud as estimated in Nakajima et al. (2003). Figure 3 shows a color-color diagram for the background stars whose fluxes were well determined in all the three bands. While the Lupus 3 dark cloud is a low-mass star forming region, the observed field contains no stars which have a clear intrinsic color excess; colors of all the stars can be explained by reddening of dwarfs or giants. We therefore assume that the color excess of the majority of the stars are totally due to extinction by dust, although stars without the J magnitude have not been examined by the color-color diagram. We compared the observed $H - K_s$ color and the surface brightness in each band toward each background star. We show the results in Figure 4. We used only stars with the color error of $\sigma_{H-K_s} < 0.14$ mag and surface brightness (i) with flux error less than 0.002 mJy arcsec⁻² and (ii) with flux larger than the 3-sigma limiting flux at each band.

There is a well defined relation between the observed $H - K_s$ color and the surface brightness for each band. A simple interpretation of the relation is as follows. Forward scattering is dominant and we consider that the starlight behind the cloud is the main source of the surface brightness in this case. Surface brightness has a peak where the column density has an adequate value so that there is enough amount of dust to scatter the incident background star light into diffuse light, while the scattered light suffers from only moderate extinction. Surface brightness is faint where the column density is small, because incident light is less scattered and therefore is less turned into diffuse light. Surface brightness is faint again where the column density is large, because incident light and scattered light suffer from heavy extinction. The value of $H - K_s$ for the peak surface brightness depends on the wavelength; at longer wavelengths the peak surface brightness takes place at higher $H - K_s$.

The surface brightness is, technically, a result of complex processes among dust grains and incident starlight, which depend on optical characteristics of dust and cloud geometry. In the followings, however, we do not take such complex physical processes into account; we consider the dark cloud as a *black box* and we try to obtain an empirical relationship

¹IRAF is distributed by the National Optical Astronomy Observatories, which are operated by the Association of Universities for Research in Astronomy, Inc., under cooperative agreement with the National Science Foundation.

² Nishiyama et al. (2006) derived the ratios of total to selective extinction in the J , H , and K_s bands toward the Galactic center with IRSF/SIRIUS. The study used a number of red clump stars toward the Galactic center region and the results are quite reliable. Relations among the V band and NIR bands which are consistent with Nishiyama et al. (2006) are not yet obtained. The results of Nishiyama et al. (2006) are significantly different from the values of Rieke & Lebofsky (1985) but are close to ones calculated from the curve No.15 of vdH. Thus, we adopted the curve No. 15 of vdH for calculations of factors for the conversions and extinction ratio in this paper.

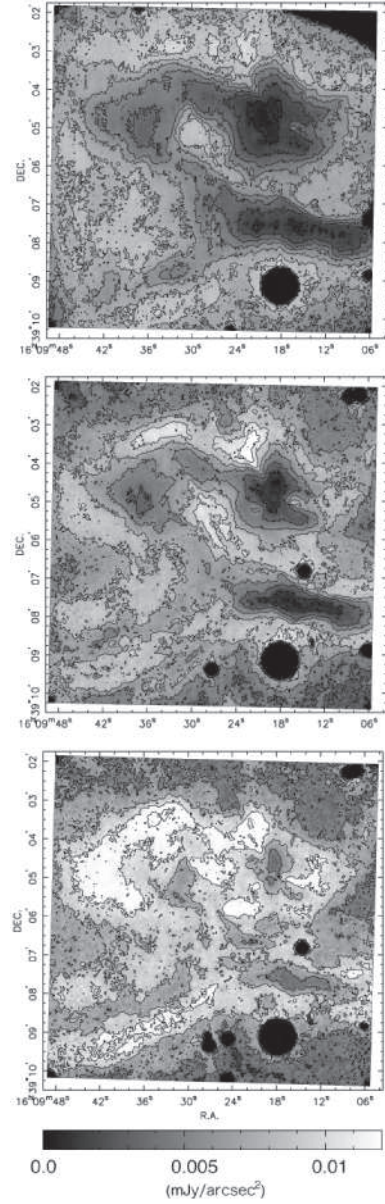


Figure 1: Surface brightness of the Lupus 3 dark cloud in the J , H , and K_s bands from top to bottom. Saturated stars are masked with circles in black. Bad pixel clusters in the J band are also shown in black. The lowest contour level denotes the 3-sigma limiting flux and the interval of contour is set to the 3-sigma limiting flux value at each band.

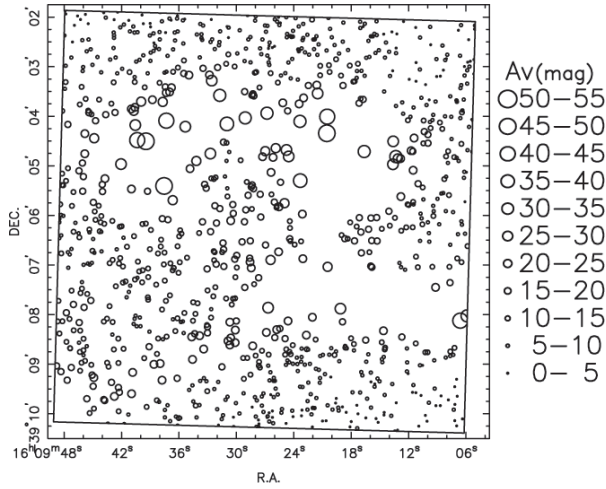


Figure 2: The A_V toward the background stars. The radius of circles represent the A_V .

between the observed $H - K_s$ color and the surface brightness for each band quantitatively and to estimate the column density based on the surface brightness toward any direction even without background stars.

We consider a simple one-dimensional scattering model to make an adequate fitting function to obtain an empirical relationship. We assume that a dark cloud is illuminated uniformly from the behind of the cloud and forward scattering is dominant at the wavelengths. When a beam of intensity I_λ passes through scattering and absorbing material of thickness ds , the radiation transfer equation for isotropic scattering is generally given by

$$dI_\lambda/ds = -(\alpha_\lambda + \sigma_\lambda)I_\lambda + \sigma_\lambda J_\lambda. \quad (1)$$

Here, α_λ is the absorption coefficient, σ_λ is the scattering coefficient, and J_λ is the mean intensity within the scattering material. We replace J_λ with $g'_\lambda I_\lambda$ based on the assumptions of one-dimensional symmetry and strong forward scattering. Here g'_λ is the probability of radiation being scattered in the forward directions. If we define

$$I(\Theta)_{scat} = \int_0^\Theta d\theta \int_0^{2\pi} d\phi I_{scat}(\theta, \phi) \sin \theta \cos \phi, \quad (2)$$

the whole radiation scattered in the forward directions, $I(\pi/2)_{scat}$, contributes to the source term due to scattering. Here, θ and ϕ are cylindrical coordinates together with the axis parallel to I_λ . The coefficient g'_λ equals to $I(\pi/2)_{scat}/I(\pi)_{scat}$. Then we get

$$dI_\lambda/ds = -\kappa_\lambda I_\lambda + g'_\lambda \gamma_\lambda \kappa_\lambda I_\lambda. \quad (3)$$

Here, $\kappa_\lambda = \alpha_\lambda + \sigma_\lambda$ is the total opacity and $\gamma_\lambda = \sigma_\lambda/(\alpha_\lambda + \sigma_\lambda)$ is the albedo.

The observed intensity of scattered radiation is then

$$I_\lambda = \int_{I_{\lambda 0}}^{J_\lambda} dI'_\lambda - I_{\lambda 0} \exp(-\tau_\lambda) = I_{\lambda 0} [\exp(g'_\lambda \gamma_\lambda \tau_\lambda) - 1] \exp(-\tau_\lambda). \quad (4)$$

Here, $I_{\lambda 0}$ is the average surface brightness of initial intensity of radiation of background stars and $\tau_\lambda = \int \kappa_\lambda ds$ is optical depth along the line of sight. Using the relationships $A_J = 4.39 E(H - K_s)$, $A_H = 2.55 E(H - K_s)$, and $A_{K_s} = 1.58 E(H - K_s)$ from the extinction curve No. 15 of vdH, we write $\tau_\lambda = 0.921 A_\lambda$ using $H - K_s$. Consequently, we get the following equation with two free parameters, $I_{\lambda 0}$ and f_d .

$$I_\lambda = I_{\lambda 0} \{ \exp[f_d \times \alpha_\lambda (H - K_s - 0.15)] - 1 \} \exp[-1 \times \alpha_\lambda (H - K_s - 0.15)] \quad (5)$$

Here, $\alpha_\lambda = \tau_\lambda/(H - K_s - 0.15)$ and equals to 4.04, 2.35 and 1.46 for J , H , and K_s , respectively. We set $(H - K_s)_{intrinsic} = 0.15$ for this equation as well as noted above. The parameter f_d represents the product of g'_λ and γ_λ .

We obtained plausible fittings to the $H - K_s$ and surface brightness relationship with the equation (5). The fitting parameters were summarized in Table 1. The thick curve denotes the best fit for each band in Figure 4. We calculated standard deviation of the surface brightness from the best fit curve for each band and obtained 0.001 mJy arcsec⁻² for all the band. The upper and lower thin curves denote the best fit curve ± 0.001 mJy arcsec⁻². We consider that the area between the two thin curves defines the empirical relationship between the surface brightness and $H - K_s$, i.e., dust column density, in the diagram for each band.

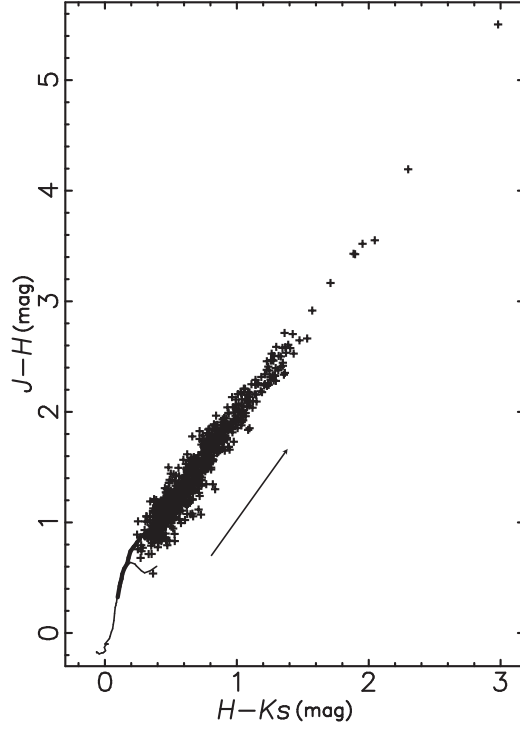


Figure 3: A $J-H$ vs. $H-K_s$ color-color diagram for the background stars. The thick and thin curves denote the loci of giants and dwarfs, respectively (Bessell & Brett 1988). The arrow is parallel to a slope of $E(J-H)/E(H-K_s)=1.7$. The length of the arrow represents an amount of reddening with $A_V=10$ mag which is calculated from vdH.

Table 1: Fitting parameters.

band	$I_{\lambda 0}$ (mJy arcsec $^{-2}$)	f_d
J	0.0123	0.808
H	0.0113	0.845
K_s	0.0133	0.889

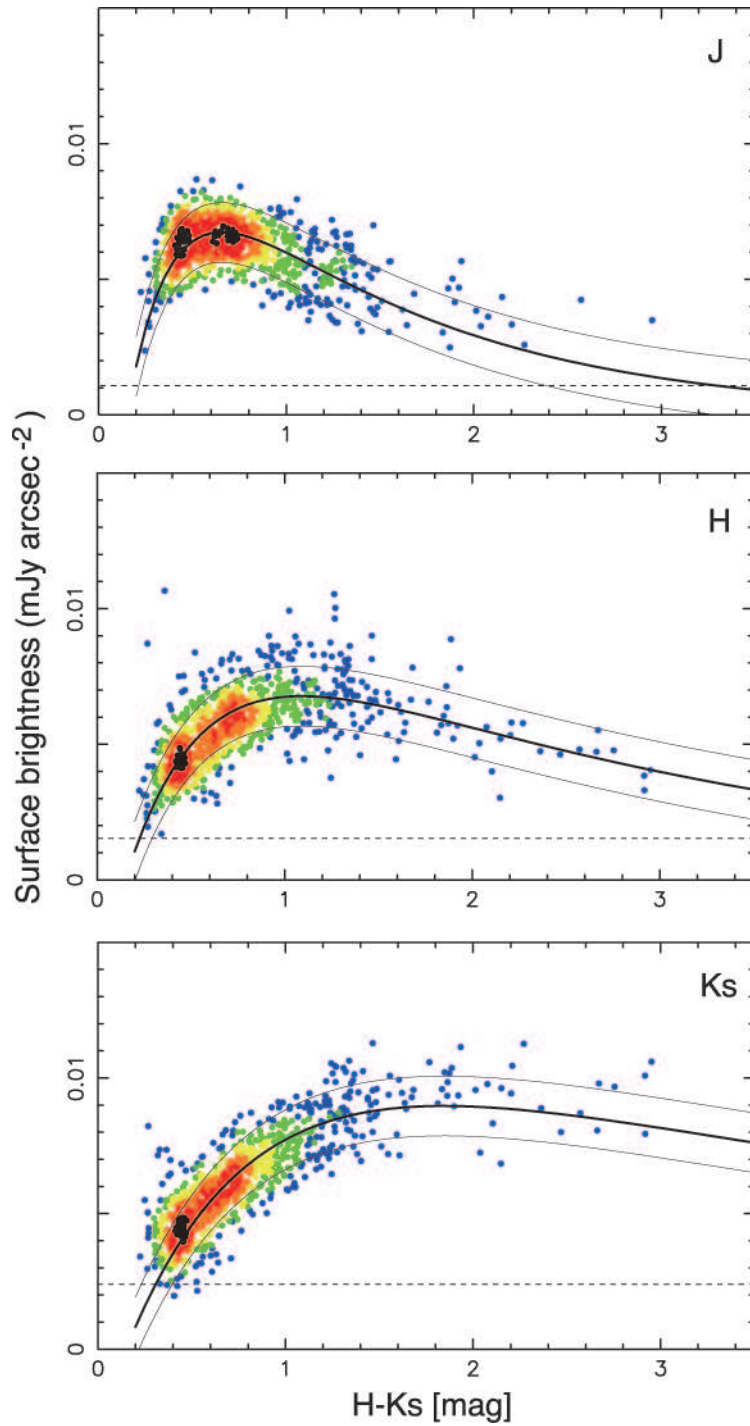


Figure 4: Relationship between $H - K_s$ and surface brightness toward background stars at J , H , and K_s . Colors of the points denote number density of the plot in the diagram; blue, green, yellow, orange, red, and black from low to high. The 3-sigma limiting fluxes are indicated by dashed lines.

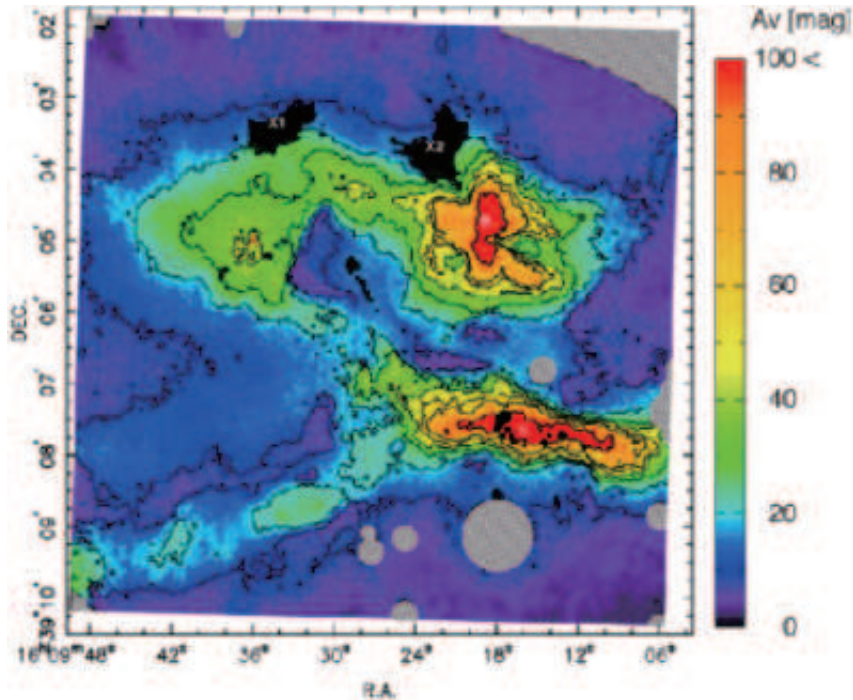


Figure 5: A_V map estimated from the surface brightnesses. Color scale indicates A_V in magnitude. The contour levels are 10, 20, 30, 40, 50, 60 and 100 mag. The pixels suffering from bad pixel clusters and saturated stars are hatched. There are three dense cores A, B, and C. The nomenclature is the same as in Nakajima et al. (2003).

3.2 Estimate of column density

We estimated a column density for each pixel from the surface brightnesses by using the equation (5) and using the parameters in Table 1. The resultant A_V map is shown in Figure 5. The procedure is as follows. Suppose that a pixel has surface brightnesses of $F_J \pm \sigma_{F_J}$, $F_H \pm \sigma_{F_H}$, and $F_{K_s} \pm \sigma_{F_{K_s}}$ at J , H , and K_s , respectively. For example, in the J band graph of Figure 4, intersections of $y = F_J$ and the empirical relationship give solutions of $x = H - K_s$ for the J band. Their errors are given by intersections of $y = F_J \pm \sigma_{F_J}$ and the curved empirical relationship band. When $y = F_J$ and the empirical relationship do not intersect but $y = F_J \pm \sigma_{F_J}$ and the curved empirical relationship band do intersect, a solution is given as the most likely point defined by the two areas; we assumed that each function has a gaussian probability distribution along the y -direction with $\sigma = \sigma_{F_J}$ or the standard deviation of $0.001 \text{ mJy arcsec}^{-2}$, and calculated the product of the two gaussians to find the point with the maximum probability in the x - y plane. We obtained solutions of $H - K_s$ for the pixel by using the surface brightnesses at H and K_s in the same method. A surface brightness can correspond to two $H - K_s$ ranges for a band, i.e., there can be two solutions, because the relationship is not monotonic but has a peak in the range considered. We checked all the possible combinations of the solutions for the J , H , and K_s bands and if the solutions for a combination are consistent with each other within their errors, we considered them as the right combination and we calculated the average of the solution and the propagated error to obtain the final solution and error of $H - K_s$ for the pixel. If the surface brightnesses for one or two bands are less than detection limit, we calculated the solutions and errors only from the other bands. Such cases occurred at areas with large extinction marked as B and C in Figure 5 and at areas with small extinction. In such cases, from the two solutions we selected the larger one for areas with large extinction and the smaller one for areas with small extinction. Consequently, we converted the $H - K_s$ to A_V by using $A_V = 18.0 \times [(H - K_s) - (H - K_s)_{\text{intrinsic}}]$ in which we set $(H - K_s)_{\text{intrinsic}} = 0.15$ as we noted above. We calculated a median of 5×5 pixels around each of pixels and set the median as the solution for the pixel. There are some clusters of pixels which have no solutions. We indicate the pixels without solutions in black in Figure 5. A pixel with a larger A_V tends to have a larger error. We calculated the mode of the error for every 5 mag bin along A_V . The median of the errors at some A_V are given in Table 2. The error is typically $\sim 30\%$.

There are two outstanding black areas at the northern edge of the dark cloud, which are indicated as X1 and X2 in Figure 5. They have no solutions of A_V , which means that the surface brightness cannot be explained by the illumination of background stars. It is possible that there are other nearby illuminating sources contributing to the

Table 2: The median of error.

A_V (mag)	median of error (mag)
10	3.5
20	6.4
30	8.0
40	11
50	14
60	17
70	21
80	25
90	28
100	33

flux of the two areas. Figure 1 shows that the two areas have the brightest flux especially in the H band. The flux of area X2 is likely attributed to the young stellar object embedded in the core B. The young stellar object is associated with HH78 and a probable jet (Nakajima et al. 2003, Teixeira, Lada, & Alves 2005). As noted in Nakajima et al. (2003), there are two possible cavity structures created by the young stellar jet. One is toward west and appears as a fan shaped local minima of $A_V \sim 30$ mag in Figure 5. The other corresponds to the area X2. The area X2 might be illuminated by the young stellar object. The illuminating source for the area X1 is not clear.

The fitting of the equation (5) is obtained from the data with $H - K_s < 3$, which means that the conversion from the surface brightnesses into A_V in the range of $A_V > 50$ mag is based on extrapolation. Therefore, the relationship is, technically, applicable only for $A_V < 50$ mag. The empirical relations tend to underestimate the J - and K_s -band surface brightnesses at high extinctions, which may also affect the reliability in the estimate of A_V at high extinctions. In order to evaluate accuracy of the fitting at high extinctions, we tried another procedure with which the fitting is more optimized at high extinctions for the J and K_s bands. We separated the data into two groups: those with $H - K_s \leq 1$ and those with $H - K_s > 1$. We searched the fitting parameters which minimize the sum of the reduced chi-squares for the two groups. We obtained the best parameters $(I_{\lambda_0}, f_d) = (0.01022, 0.8083)$ and $(0.0098, 0.9654)$ for J and K_s , respectively. Constant of 0.001 mJy arcsec $^{-2}$ was needed to add the equation (5) for the best fittings for both J and K_s . The resultant relations do not underestimate the surface brightnesses at J and K_s . We calculated the difference of A_V between this fitting procedure and the former one for each pixel. In a range of $0 \leq A_V \leq 50$, the fraction of pixels which have the difference of A_V less than A_V error is 96%. The fraction is 54% and 16% in ranges of $50 \leq A_V \leq 100$ and $100 \leq A_V \leq 150$, respectively. Thus, the estimated A_V and error are marginally unreliable in ranges of $50 \leq A_V \leq 100$ and completely unreliable for $100 \leq A_V \leq 150$.

Figure 6 shows the relationship between the A_V estimated from the surface brightnesses and that from $H - K_s$ of background stars, in other words, a comparison of Figures 2 and 5. There is a slight tendency that A_V estimated from the background stars is larger than that from the surface brightnesses. A least square fit yields a slope of 1.05 for the relationship. This may be due to the shadowing effects produced by optically thick regions (Juvela et al. 2006). However, the deviation of 5 % is not significant compared to the typical error of 30 % for the A_V estimate with the surface brightnesses.

3.3 Fitting parameters

We made a simple one-dimensional formula with two parameters. In reality, however, the observed cloud is not one-dimensional, and the scattered source term in the equation (3) is to be altered according to the local cloud density structure and radiation field. In this study, the derivation of column densities is essentially empirical. The fitted values of the parameters do not necessarily match the actual physical parameters: intensity of background radiation and dust properties. Here, we examine the fitted values.

We compared the fitting parameter I_{λ_0} and the average surface brightness from the background stars for each band. We made a K_s band luminosity function of the point sources with $A_{K_s} \leq 1.0$ mag, in which magnitude was de-reddened by $K_{s0} = K_s - 1.58(H - K_s - 0.15)$. The log of the luminosity function is well fitted by a power-law in the magnitude range of $10 \leq K_s \leq 17$. We calculated a total flux from the de-reddened K_s magnitude between $10 \leq K_s \leq 17$. In order to correct the total flux by taking the fainter stars into account, we also estimated the flux contributed by background stars with $17 \leq K_s \leq 30$ by integrating the power-law fitting function. Then we divided the total flux by the area of $H - K_s \leq 0.78$ which is estimated by the A_V map in Figure 5. The color of $H - K_s = 0.78$

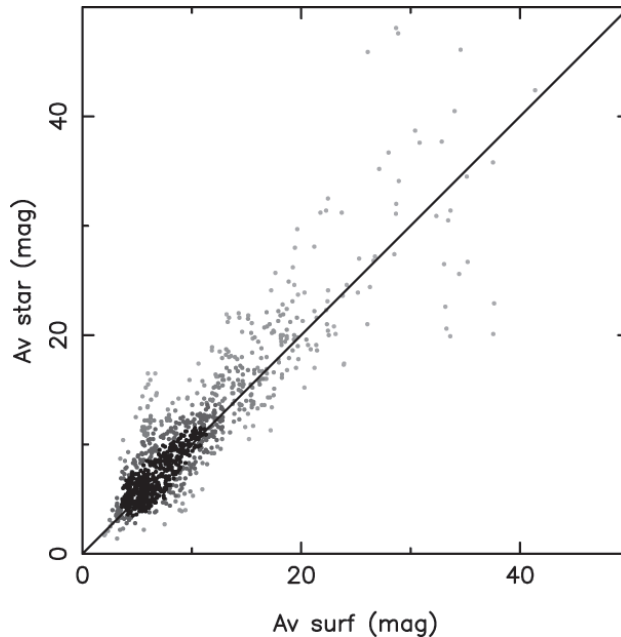


Figure 6: Relationship between the A_V estimated from the surface brightnesses and that from $H - K_s$ of background stars. The grayscale of the points are assigned according to the number density on the graph; darker for higher density. The solid line has a slope of 1.

corresponds to $A_{K_s} = 1.0$ mag. We obtained $0.011 \text{ mJy arcsec}^{-2}$, with an uncertainty of a factor of 2, as the average flux at K_s from the background stars. Similarly, we estimated the average flux at H to be $0.011 \text{ mJy arcsec}^{-2}$. Thus, the fitting parameter I_{λ_0} is consistent with the average flux from the background stars in the H and K_s band. We could not obtain a meaningful value of the average flux for the J band, because the number of the stars with $A_J \leq 1.0$ mag is too small and the luminosity function was not fitted by a power-law function.

The parameter f_d is a product of γ_λ and g'_λ : the albedo and the probability of radiation being scattered into the forward direction. Both γ_λ and g'_λ range between 0 and 1. The resultant values of $f_d = 0.81\text{-}0.89$ means that both the parameters have values close to the upper limit. This is consistent with large albedo obtained in Nakajima et al. (2003).

3.4 Comparison with the previous studies

Padoan et al. (2006) and Juvela et al. (2006, 2008) developed a new method of mapping column density of dark cloud using NIR scattered light. This paper is based on the similar considerations; however, this paper has some new aspects. Our method uses an empirical formula whose parameters are directly calibrated by the color excess of the background stars, while the previous studies used an analytic formula and used an extinction map derived from the color excess just for comparison as an independent tracer. We do not use a smoothed extinction map but the color excess of individual stars for comparison with the surface brightness toward each star. The use of individual background stars avoids the problems with the bias when there are few background stars (Juvela et al. 2008). By adopting a different formula, our method covers a part beyond the point where surface brightness starts to decrease with increasing column density, while the previous studies did for only the non-saturated part of the relation.

3.5 Other remarks

When this method is applied to other clouds, the fitting parameters should be determined for each cloud. The fitting parameters for each band in the equation (5) can be different among dark clouds. The parameter I_0 represents the average surface brightness of background stars, which depends on the Galactic coordinates. The parameter f_d represents optical property of dust grain in the cloud, which can be different among the clouds.

Teixeira, Lada, & Alves (2005) made an extinction map toward the Lupus 3 dark cloud with the $H - K_s$ color of the background stars. While their map generally agrees with ours (see their Figure 2 and 6) in their smoothing scale, 30 and 40 arcsec, the map failed to trace the core C (the core E in their paper) properly due to the lack of stars.

4 Conclusion

We constructed an empirical relationship equation between the surface brightness and column density of the Lupus 3 dark cloud for each J , H , and K_s band. By using the equations, we obtained a column density map with a pixel scale of 2.3×2.3 arcsec² and a large dynamic range up to $A_V = 50$ mag of the cloud from the NIR surface brightness. We expect the empirical method to be one of the new tools of column density mapping of dark clouds.

5 Acknowledgment

We thank the anonymous referee for the constructive comments. We thank Dr. Daisuke Kato for his comments. RK and MT are supported by Grants-in-Aid from the Ministry of Education, Culture, Sports, Science and Technology (No 16340061). This publication makes use of data products from the Two Micron All Sky Survey, which is a joint project of the University of Massachusetts and the Infrared Processing and Analysis Center/California Institute of Technology, funded by the National Aeronautics and Space Administration and the National Science Foundation.

References

- [1] Bessell, M. S. & Brett, J.M. 1988, PASP, 100, 1134
- [2] Foster, J. & Goodman A. 2006, ApJ, 636, L105
- [3] Juvela, M et al. 2006, A&A, 457, 877
- [4] Juvela, M et al. 2008, A&A, 480, 445
- [5] Lehtinen, K., & Mattila, K. 1996, A&A, 309, 570
- [6] Nakajima, Y. et al. 2003, AJ, 125, 1407
- [7] Nakajima, Y. et al. 2008, PASP, in submitted
- [8] Nishiyama, S. et al. 2006, ApJ, 638, 839
- [9] Padoan, P, Juvela, M., & Pelkonen, V.-M., 2006, ApJ, 636, L101
- [10] Rieke, G.H. & Lebofsky, M.J. 1985, ApJ, 288, 618
- [11] Teixeira, P. S, Lada, C. J. & Alves, J. F. 2005, ApJ, 629, 276
- [12] van de Hulst, H.C. 1946, Rech. Astron. Obs. Utrecht, 11, 2